Title

Neuropathologic Heterogeneity Does Not Impair Florbetapir-Positron Emission Tomography Postmortem Correlates

Journal

Journal of Neuropathology & Experimental Neurology, 73(1)

ISSN

0022-3069

Authors

Dugger, Brittany N
Clark, Christopher M
Serrano, Geidy
et al.

Publication Date

2014

DOI

10.1097/nen.0000000000000028

Peer reviewed

Published in final edited form as:
J Neuropathol Exp Neurol. 2014 January ; 73(1): 72–80. doi:10.1097/NEN.0000000000000028.

Neuropathologic Heterogeneity Does Not Impair Florbetapir-PET Postmortem Correlates

Brittany N. Dugger, PhD[b], **Christopher M. Clark, MD**[a,†], **Geidy Serrano, PhD**[b], **Monica Mariner, BS**[b], **Barry J. Bedell, MD PhD**[c], **R. Edward Coleman, MD**[d,†], **P. Murali Doraiswamy, MBBS**[d], **Ming Lu**[a], **Adam S. Fleisher, MD MAS**[e], **Eric M. Reiman, MD**[e], **Marwan N. Sabbagh, MD**[b], **Carl H. Sadowsky, MD**[f], **Julie A. Schneider, MD**[g], **Simone P. Zehntner, PhD**[c], **Alan P. Carpenter, PhD**[a], **Abhinay D. Joshi, PhD**[a], **Mark A. Mintun, MD**[a], **Michael J. Pontecorvo, PhD**[a], **Daniel M. Skovronsky, MD PhD**[a], **Lucia I. Sue, BS**[b], and **Thomas G. Beach, MD PhD**[b]

[a]Avid Radiopharmaceuticals, Philadelphia, PA

[b]Banner Sun Health Research Institute, Sun City, Arizona

[c]Biospective Inc., Montreal, Canada; Montreal Neurological Institute, McGill University, Montreal, Canada

Correspondence: Thomas G. Beach, Banner Sun Health Research Institute, 10515 West Santa Fe Drive, Sun City, AZ 85351, USA, Telephone: 623-832-5643, Fax: 623-832-2967, Thomas.beach@bannerhealth.com.
†Drs. Clark and Coleman died in January, 2012 and June, 2012; respectively.

Conflicts of Interest

BND, GES, MM, and LIS have had portions of their salary supported by Avid Radiopharmaceuticals, a division of Eli Lily. CMC, MJP, APC, ADJ, MAM, and DMS are or were employees of Avid Radiopharmaceuticals, a division of Eli Lilly, and formerly held Avid stock or options. TGB has received funding related to the topic of this report from the National Institute on Aging (grant P30 AG19610), Arizona Department of Health Services (contract 211002 awarded to the Arizona Alzheimer's Research Center), Avid Radiopharmaceuticals, Bayer Healthcare, and GE Healthcare. BJB and SPZ have received compensation and shares from Biospective. REC reports membership of the medical advisory board for GE Healthcare from 2003 to 2008; being a consultant for GE Healthcare from 2003 to 2008; receiving a research grant from GE Healthcare in 2010; receiving funding for a clinical trial from Molecular Insights Pharmaceuticals in 2010; serving on a medical advisory board for Molecular Insights Pharmaceuticals from 2004 to 2009; serving on a medical advisory board and receiving a grant from Avid to support his participation in this study; serving on a medical advisory board and as a consultant to Eli Lilly; and serving on a medical advisory board for Bayer. PMD reports receiving research grants related to this project (awarded to Duke University), currently or previously serving as an adviser to Piramal, Targacept, Abbvie, Danone, Cognoptix, Baxter, Forest, Bristol-Myers Squibb, Avid Radiopharmaceuticals, Lundbeck, Medivation, Pfizer, Elan, Eli Lilly, Bayer, Neuroptix, Neuronetrix, Sonexa, Accera, TauRx, Myriad, National Institute on Aging, AstraZeneca, Labopharm, Clarimedix, National Institute of Mental Health, National Institute of Neurological Disorders and Stroke, Alzheimer's Association, Alzheimer's Foundation, Rutgers University, and the University of California; owning stock in Sonexa and Clarimedix; and receiving a grant from Avid (awarded to Duke University) for his participation in this study. ASF has served as a consultant to Lilly and Avid, and received grant funding from Avid. EMR reports serving as a scientific adviser to Sygnis, AstraZeneca, Bayer, Eisai, Elan, Eli Lilly, GlaxoSmithKline, Intellect, Link Medicine, Novartis, Siemens, and Takeda; having had research contracts with National Institute on Aging, Arizona Department of Health Services, AstraZeneca and Avid; having patents pending for an imaging strategy for screening treatments for Alzheimer's disease in laboratory animals, a biomarker strategy for the assessment of presymptomatic treatments for Alzheimer's disease, a statistical strategy for the analysis of complementary complex datasets, and *GAB2* testing in clinical assessment of Alzheimer's disease through TGen, AstraZeneca, Avid Radiopharmaceuticals, and Kronos Life Sciences; receiving research grants from the National Institute on Aging, National Institute for Mental Health, an anonymous foundation, Nomis Foundation, Banner Alzheimer's Foundation, and State of Arizona; holding patents for an imaging strategy for the screening of AD treatments in laboratory animals (active), a biomarker strategy for the assessment of presymptomatic treatments for Alzheimer's disease (pending, through Banner Health), a statistical strategy for the analysis of complementary complex data sets (pending, through Banner Health), and GAB2 testing in clinical assessment of Alzheimer's disease (pending, through Translational Genomics Research Institute); and serving as the executive director for the Banner Alzheimer's Institute and the director of the Arizona Alzheimer's Consortium. MNS reports serving in a consulting or advisory capacity for Eli Lilly, Amerisciences, Takeda, Eisai, Pfizer, GlaxoSmithKline; receiving royalties from Wiley, FT Pearson Press, and Amerisciences; and receiving contracts and grants from Celgene, Ceregene, Bayer, Baxter, Bristol-Myers Squibb, GE Healthcare, Eli Lilly, Pfizer, Wyeth, Janssen, Elan, Avid, Genentech, Medivation, and Eisai. CHS reports serving on speaker bureaus for Novartis, Forest, and Accera, and as a consultant to Novartis and Eli Lilly. JAS reports being a consultant for Avid Radiopharmaceuticals and serving in an advisory capacity for Eli Lilly and GE Healthcare receiving compensation for services.

[d]Duke University Medical Center, Durham, NC

[e]Banner Alzheimer's Institute, Phoenix, AZ

[f]Nova SE University, Ft. Lauderdale, FL

[g]Rush University Medical Center, Chicago, Illinois

Abstract

Neuropathologic heterogeneity is often present within Alzheimer's disease (AD). We sought to determine if amyloid imaging measures of AD are affected by concurrent pathologies. Thirty-eight clinicopathologically-defined AD and 17 non-demented cases (ND) with quantitative florbetapir F-18 (^{18}F-AV-45) PET imaging during life and histological β-amyloid quantification and neuropathologic examination were assessed. AD cases were divided on the basis of concurrent pathologies, including those with Lewy bodies (N=21), white matter rarefaction (N=27), severe cerebral amyloid angiopathy (N=11), argyrophilic grains (N=5) and TDP-43 inclusions (N=18). Many cases exhibited more than one type of concurrent pathology. The ratio of cortical to cerebellar amyloid imaging signal (SUVr) and immunohistochemical β-amyloid load were analyzed in six cortical regions of interest. All AD subgroups had strong and significant correlations between SUVr and histological β-amyloid measures (p values <0.001). All AD subgroups had significantly greater amyloid measures compared to ND, and mean amyloid measures did not significantly differ between AD subgroups. When comparing AD cases with and without each pathology, AD cases with Lewy bodies had significantly decreased SUVr measures compared to AD cases without (p = 0.002); there were no other paired comparison differences. These findings indicate florbetapir-PET imaging is not confounded by neuropathological heterogeneity within AD.

Keywords

argyrophilic grains; autopsy; cerebral amyloid angiopathy; Lewy bodies; plaques; TDP-43; vascular dementia; white matter; leuko-araiosis

INTRODUCTION

Biomarkers are increasingly being regarded as essential tools for drug discovery and for monitoring the effects of therapeutic agents for neurodegenerative diseases. In less than 10 years since the first publication, positron emission tomography (PET) imaging of brain amyloid with Pittsburgh Compound-B, ^{11}C-PiB, has become an important research tool (1). However, the 20 minute half-life of ^{11}C -PiB restricts its usage to specialized research centers in close proximity to a biomedical cyclotron (1). In contrast, labeling with ^{18}F gives a half-life of 110 minutes (2) and numerous ligands are currently under study utilizing this approach (3–10). One such ^{18}F-labeled compound, florbetapir F-18 (^{18}F-AV-45), has been shown, in an autopsy study of 35 subjects that was later extended to 59 subjects, to have high sensitivity and specificity for β-amyloid (8, 11, 12). However, detailed neuropathological examinations of these subjects have not yet been published.

Considerable neuropathologic heterogeneity is often present in persons with AD and other forms of dementia, raising the question as to whether this might have effects on amyloid imaging measures. This may be especially crucial since the clinical diagnosis of autopsy confirmed AD may be incorrect in between 20–30% of subjects (13) and amyloid imaging is expected to enhance this. AD is pathologically defined by plaques and tangles but a large majority of AD cases have a variety of concurrent pathologies including Lewy bodies, vascular lesions, argyrophilic grains and TDP-43 inclusions (14–19).

The purpose of the present study was to test the hypothesis that florbetapir F-18 PET imaging is a reliable method for estimating *in vivo* cortical amyloid load in AD subjects regardless of neuropathologic heterogeneity. This autopsy series is the first to describe the full spectrum of neuropathological findings in AD subjects who had received amyloid imaging during life. We included AD and non-demented cases from the previously published reports, (8, 11) dividing the pathologically-defined AD subjects into subgroups based on some of the major concurrent pathologies found within AD. These subgroups consisted of those with Lewy bodies (LBs), white matter rarefaction (WMR), severe cerebral amyloid angiopathy (CAA), argyrophilic grains (Arg) and phosphorylated TAR DNA binding protein-43 (TDP-43) inclusions. We examined whether *in vivo* amyloid imaging measures of AD subjects, or their correlates with postmortem histological β-amyloid measures, varied due to the presence or absence of these concurrent pathologies.

MATERIALS AND METHODS

Subject selection

Subjects were derived from those described in two previous publications (8, 11). Details of the recruitment, amyloid imaging, tissue processing, and analytic methodology are given in the prior publications. Briefly, patients near the end of their lives were recruited from hospice, long-term care and community healthcare facilities for florbetapir-PET scanning. Fifty-nine subjects died within two years of amyloid imaging, were autopsied and neuropathologically examined. From these, 55 subjects were selected for inclusion in the present study, based on their clinicopathological classification as either AD or non-demented controls. Subjects with AD (N=38) were defined as demented subjects meeting CERAD “probable” or “definite” criteria for AD pathology (22). Control cases (N = 17, Table 1) were defined as those without a final clinical diagnosis of dementia (regardless of pathology findings), and included clinically-normal non-demented individuals (N = 12) and those with mild cognitive impairment (MCI, N = 5) but not demented subjects. Three other subjects were excluded because they were demented but did not meet neuropathological criteria for AD; these included one with Parkinson’s disease, one with dementia with Lewy bodies (DLB) and one with hippocampal sclerosis dementia. One case was excluded due to methodological deviation.

Florbetapir-PET imaging methods

The details of the imaging methods have been previously described (8, 11). Briefly, each subject underwent a 10-minute PET scan at 50 minutes after receiving an intravenous bolus of 370 MBq (10mCi) florbetapir F-18. Acquired PET scans were reconstructed either by

iterative reconstruction with a post-reconstruction Gaussian filter or row action maximum likelihood algorithms to a 128×128 matrix with a zoom of 2.0– 2.33. Florbetapir F18 PET images were independently spatially normalized using statistical parametric mapping to standard atlas co-ordinates with reference to a florbetapir PET template. Standard uptake value ratios (SUVr) were expressed as the average ratio, compared to the whole cerebellar uptake, of 6 predefined anatomically relevant cortical regions: frontal, parietal, temporal, precuneus, posterior cingulate and anterior cingulate cortices.

Histological amyloid quantification

Upon autopsy, brains were processed with methods as outlined previously (8, 11), as well as with standard methods utilized by the Banner Sun Health Research Institute Brain and Body Donation Program (20). Brains were fixed whole in 10% neutral-buffered formalin for 2 weeks prior to dissection. One set of tissue blocks was taken from the same ROIs as were used for imaging (8). These blocks were embedded in paraffin and immunohistochemically stained for β-amyloid using the anti-Aβ antibody 4G8 (Covance, Emeryville, CA)(8). The cortical amyloid burden on each of these slides, which included all morphologically-defined plaque subtypes, was defined as the percentage of gray matter occupied by stained neuropil exceeding a threshold stain density (8, 21), using PERMITS™ image processing and analysis software (Biospective Inc., Montreal, Quebec, Canada). Amyloid burden estimates were thus obtained for all six cortical regions of interest (ROIs), and a mean cortical amyloid load was determined by averaging these. Additionally, another set of large (3 × 5 cm) tissue blocks, from standard levels of the frontal (superior half of frontal lobe at the coronal level of the genu of the corpus callosum), parietal (superior half of parietal lobe at the coronal level of the splenium of the corpus callosum) and temporal lobes (coronal levels of the amygdala and body of the hippocampus), were cryoprotected in ethylene glycol and sectioned at 80 μm thickness on a sliding freezing microtome (20). These sections were stained using the Campbell-Switzer stain, an enhanced, amyloid-selective silver technique, together with the Thioflavin S stain; semi-quantitative estimates of regional and average (means from all three regions) cortical amyloid burden were obtained from these sections. Scores for plaque density were derived by considering all types of plaques (cored, neuritic and diffuse) together to obtain a “total” plaque score, while cored and neuritic plaques were also separately estimated. Plaque density scores were obtained by assigning values of none, sparse, moderate and frequent, according to the published CERAD templates (22, 23). Conversion of the descriptive terms to numerical values resulted in scores of 0–3 for each area (demonstrated in Figure 1). Semi-quantitative amyloid scoring was performed blinded to clinical diagnosis by a single observer (TGB).

Neuropathological examination

Neuropathological examination was performed blinded to clinical diagnosis by a single observer (TGB); assignment of a clinicopathological diagnosis was done after un-blinding to clinical history. Multiple additional brain regions were dissected for neuropathological assessment and diagnosis according to the standard protocols of the Banner Sun Health Research Institute Brain and Body Donation Program (20). This included a comprehensive set of twenty-two blocks embedded in paraffin as well as a set of six to eight 3 × 5 cm blocks from standard levels of the frontal, temporal and parietal lobes as described above, as

well as one block through the middle of the occipital lobe and one parasagittal block through the cerebellum at the level of the dentate nucleus. The temporal and parietal blocks contained standard levels of the thalamus, basal ganglia and substantia nigra. These cryoprotected blocks were sectioned at 80 μm thickness on a sliding freezing microtome and stained with H & E, Thioflavin S and enhanced silver methods (Campbell-Switzer and Gallyas) for amyloid plaques and neurofibrillary tangles. Amyloid plaque and neurofibrillary tangle density and distribution were determined in these thick sections of the frontal, temporal, parietal and occipital cortex as well as hippocampus and entorhinal cortex, based on the CERAD templates (23) and the aggregate impression from Thioflavin S, Campbell-Switzer and Gallyas methods. Amyloid plaque distribution was described according to the Thal-Braak system while the distribution of neurofibrillary degeneration was described using the original Braak protocol; for both of these, their development was based on the usage of similarly-thick sections (24, 25). As in the originally-published studies of this group of subjects, the diagnosis of AD was based on a CERAD “probable” or “definite” classification (23).

Rating of white matter rarefaction (WMR; Figure 1) was done using a semi-quantitative (0–3) scale on the thick 80 μm sections stained with H & E, according to the fraction of centrum semi-ovale affected (20). Those cases with a score of 2 or higher in one or more lobes were considered to have significant WMR. Cerebral amyloid angiopathy (CAA) was defined semi-quantitatively with three levels of severity by analogy to the CERAD templates; for this study, significant CAA was defined when one or more cerebral lobes had a severity score of 2 or higher. Argyrophilic grains (Arg) were defined as typical spindle-shaped structures revealed by the Gallyas silver stain (26, 27) and were recorded as being present or absent.

Formalin-fixed, paraffin-embedded sections from a set of ten standard brain regions (28) were immunohistochemically stained with an antibody against phosphorylated α-synuclein peptide (1:10,000; rabbit polyclonal anti-human phosphoserine 129, gift of Dr. Haruhiko Akiyama, Tokyo Institute of Psychiatry, Tokyo, Japan) (29) and these were used to classify the density and distribution of Lewy bodies and related neuropil elements using the Unified Staging System for Lewy Body Disorders (28). Diagnostic criteria for dementia with Lewy bodies were those of the third Dementia with Lewy Bodies Consortium (14); the diagnosis was assigned when subjects met “intermediate” or “high” definitions.

Thick, free-floating 80 μm sections of the frontal and temporal lobes were immunohistochemically stained with an antibody against phosphorylated TDP-43 peptide (1:10,000 rabbit polyclonal antihuman phosphoserine 409/410, gift of Dr. Haruhiko Akiyama, Tokyo Institute of Psychiatry, Tokyo, Japan) (30). Diagnostic criteria for vascular dementia were adapted from those of Roman et al. (31).

Statistical methods

Statistical analyses and graphs were performed with Sigma Plot 12.1 (Systat Software, Inc. San Jose, CA) and Microsoft Excel (Microsoft Corporation, Redmond, WA). The Student t-test and the Mann-Whitney U-test were used to compare group means for continuous and discontinuous measures, respectively. Chi-squared and Fisher’s exact tests were used to

determine whether proportional measures were significantly different. Spearman correlations were used to show relationships between semi-quantitative measures. For all tests, the type I error rate was set as 0.05. For multiple comparisons, the Benjamini-Hochberg False Discovery Rate Procedure was applied to control the expected proportion of falsely rejected hypotheses.

RESULTS

Table 1 shows the complete list of AD cases and their concurrent pathologies. Of the AD cases, 21 had Lewy body-related α-synuclein pathology (LBs); 8 met clinicopathological criteria for dementia with Lewy bodies, 27 had significant WMR, 11 had significant CAA, 5 had Arg, and 18 had incidental TDP-43 inclusions. Furthermore, one AD case had an additional diagnosis of Trisomy 21 and one had concomitant frontotemporal lobar degeneration with TDP-43 inclusions (FTLD- TDP). There was considerable overlap, with many cases exhibiting more than one type of concurrent pathology. Only three AD cases did not have any of the above concurrent diagnoses (“pure” AD). In all groups (AD subsets and non-demented individuals) there were multiple cases with one or more infarcts (38% of the non-demented cases and 39% of the AD subjects had one or more infarcts). We did not analyze for the effect of infarcts on amyloid measures due to great variability in infarct size, location and type. Table 2 summarizes the overall group demographics. Groups did not significantly differ from each other with respect to age of death, interval from imaging until death, or gender ratio. All AD subgroups had significantly higher CERAD neuritic plaque densities, as well as higher Braak NFT stages when compared with the MCI and non-demented control group (p values < 0.001), but did not significantly differ from each other in these measures. In terms of both *in vivo* imaging-derived SUVr and postmortem β-amyloid IHC measures, when adjusting for multiple comparisons, all AD subgroups were significantly different from the normal control and MCI groups ($p < 0.001$), but there were no significant differences amongst the subgroups. There were no statistically significant differences on any measure between MCI and non-demented individuals. Unadjusted p-values generated by comparisons of SUVr and β-amyloid IHC values of each AD subgroup are located in Table 3. The only significant difference was in SUVr measures between AD with LBs and AD with CAA ($P = 0.045$).

There were significant correlations between cortical amyloid measures (SUVr and β-amyloid IHC) and both Braak neurofibrillary stage and Thal-Braak amyloid phase. Correlation coefficients (Spearman rho) for Braak NFT stage with SUVr and β-amyloid IHC measures were 0.709 and 0.717 respectively (p values < 0.0001). Correlation coefficients for Thal-Braak amyloid phase to SUVr and β-amyloid IHC measures were 0.792 and 0.826 respectively (p values < 0.0001).

The case-by-case *in vivo* estimates of amyloid density, based on the florbetapir PET image average cortical to cerebellum standard uptake value ratio (SUVr), for each AD subgroup are located in Figure 2. The figure shows that for each AD subgroup individual cases were within the range predicted from the overall AD population. When conducting a pairwise comparison of AD cases with and without each concurrent pathology; AD cases with LBs

were significantly different from AD cases without LBs ($p = 0.002$; Fig. 3). All other comparisons showed no significant differences.

In vivo average cortical amyloid load (SUVr) was significantly correlated with postmortem average cortical β-amyloid load (IHC) across all study subjects (including both control and AD cases) regardless of co-morbid pathology. Correlation coefficients (Spearman rho) were 0.76 for AD cases with WMR ($p < 0.0001$), 0.78 for AD cases with LBs ($p < 0.0001$), 0.60 for AD cases with Arg ($p = 0.003$), 0.76 for cases with severe CAA ($p = 0.0006$) and 0.78 for AD cases with TDP-43 inclusions ($p = 0.0003$). For the entire AD group the correlation coefficient was 0.71 ($p < 0.001$). When considering all cases together, using semi-quantitative estimates of average cortical amyloid plaque densities derived from the Campbell-Switzer silver stain and Thioflavin S stain, the correlation coefficient (Spearman rho) was 0.76 for the comparison with average cortical β-amyloid IHC ($p < 0.0001$), and 0.73 for the comparison with SUVr ($p < 0.0001$). MCI and non-demented control subjects were included in all correlations in order to attain a wider range of measures.

DISCUSSION

There is great interest in validating amyloid imaging methods as they hold great promise for improving AD clinical diagnostic accuracy and for testing of disease-modifying agents. We have recently published results from PET studies using the amyloid ligand, florbetapir F-18, demonstrating a strong correlation between *in vivo* and postmortem amyloid load estimates in the cerebral cortex, utilizing Alzheimer's disease subjects as well as non-demented individuals (8, 11). These previous results found florbetapir-PET images rated as positive or negative for amyloid presence agreed, in 55 of 59 individuals, with postmortem histology for the presence or absence of a defined amyloid plaque density (11). However, the detailed neuropathology of these cases has not been published and is of considerable interest as AD is neuropathologically heterogeneous. We sought to determine whether amyloid imaging measures differed or had differing *in vivo*-postmortem correlation strength depending on the type of concurrent pathologies within AD. The 38 AD subjects in this study, which were selected from the original study group of 59 subjects (8), had a high frequency of other pathologies including LBs, WMR, severe CAA, Arg and TDP-43. There were only three AD cases that did not contain at least one of these additional abnormalities, supporting the evolving consensus that AD is more frequently than not complicated by additional pathology (16–19). Despite this neuropathological heterogeneity, *in vivo* imaging measures of average cortical β-amyloid load (SUVr) remained significantly correlated to average cortical postmortem β-amyloid IHC measures within all AD pathology subgroups. All AD cases except one had mean cortical SUVr values that were above the proposed cutoff "positive" ratio of 1.1 (Fig. 2) (32). The one positive case, based on histology (case #24 in Table 1), that was below the cutoff ratio had multiple concomitant pathologies including hippocampal sclerosis, TDP-43 inclusions; Arg, WMR, and LBs. There are no clear conclusions as to why this case is below the proposed cutoff and it is possible that it is only random variation. Furthermore, both *in vivo* and postmortem average cortical amyloid measures for each AD subgroup were significantly greater than those for non-demented individuals and the average SUVR values of each AD subgroup stay close to the overall mean. Overall, these data suggest that florbetapir SUVr measures are a reliable predictor of

postmortem histopathological β-amyloid load despite the substantial neuropathological variability commonly encountered in AD subjects.

This study contributes new clinicopathological correlative data for subjects that have received amyloid imaging during life. In particular, we are not aware of any reports that have described *in vivo* amyloid imaging results for AD with concurrent WMR, Arg or aberrant TDP-43 deposition (26, 33). Amyloid imaging results for subjects with clinically-diagnosed Lewy body disorders have been published, but these studies have generally lacked postmortem confirmation and the clinical diagnostic accuracy for DLB has known limitations (34–41). To our knowledge there has only been one small series and one case study with autopsy confirmation of DLB (36, 37). In the case study, there was a strong association between PiB retention and postmortem cortical β-amyloid densities in 17 corresponding ROIs (36). In a series of 5 clinically diagnosed Parkinson's dementia and DLB cases that had come to autopsy, three cases were PiB positive and all had amyloid pathology at autopsy; one of these cases also met neuropathological diagnostic criteria for AD. Neither of the two PiB negative cases had significant amyloid pathology at autopsy (37). No amyloid imaging study has compared clinicopathological AD cases with and without LBs. Our results demonstrated that AD cases with LBs had significantly decreased SUVr measures compared to AD cases without LBs; additionally, the only significantly different comparison, out of all possible comparisons, of average cortical SUVr between all AD subgroups, was between the AD/CAA subgroup and the AD/LB subgroup, and again, the AD/LB subgroup had a lower average cortical SUVr. These results are consistent with previous neuropathological reports demonstrating plaque densities may be lower in the cortex of AD subjects with DLB as compared to AD subjects without DLB (14, 38,42, 43). High densities of CAA are likely to be additive to amyloid plaques in affecting cortical SUVr, as a high-resolution postmortem study has demonstrated that another amyloid imaging agent, PiB, binds with high sensitivity to CAA (44). However, we found no significant differences in average cortical SUVr between AD cases with and without higher CAA density.

Our study had some limitations. One limitation is subjects tended to have either no amyloid or high amyloid loads, with relatively few having sparse to moderate loads. This is most likely due to the clinical trial selection process, whereby most subjects were identified by neurologists with an interest in dementia, and by the need to select subjects who were near death. Amyloid deposition in AD is hypothesized to be a rapid and mostly preclinical event (45). To enhance the range of amyloid densities we therefore included the non-demented study individuals. Another limitation is the relatively low number of subjects. Although this is the largest amyloid imaging-to-autopsy study to date, our sample size is still relatively small, especially when subdivided into several subgroups. Furthermore, many cases exhibited more than one type of concurrent pathology. Still, this is a real life setting for AD subjects and most AD subjects will have more than one additional non-AD pathology. The main purpose of this study was to examine whether quantitative cortical amyloid imaging measures differed as a result of neuropathological heterogeneity within AD. The results show that despite considerable neuropathological diversity, cortical amyloid imaging measures were remarkably uniform. In conclusion, the results of this study indicate that

florbetapir PET-derived estimates of AD cortical amyloid load are not significantly altered by several common concomitant pathologies.

Acknowledgments

Data utilized in this study was obtained through funds provided by Avid Radiopharmaceuticals. The Brain and Body Donation Program is supported by the National Institute of Neurological Disorders and Stroke (U24 NS072026 National Brain and Tissue Resource for Parkinson's Disease and Related Disorders), the National Institute on Aging (P30 AG19610 Arizona Alzheimer's Disease Core Center), the Arizona Department of Health Services (contract 211002, Arizona Alzheimer's Research Center), the Arizona Biomedical Research Commission (contracts 4001, 0011, 05-901 and 1001 to the Arizona Parkinson's Disease Consortium) and the Michael J. Fox Foundation for Parkinson's Research.

Disclosure of Funding Data utilized in this study was obtained through funds provided by Avid Radiopharmaceuticals. The Brain and Body Donation Program is supported by the National Institute of Neurological Disorders and Stroke (U24 NS072026 National Brain and Tissue Resource for Parkinson's Disease and Related Disorders), the National Institute on Aging (P30 AG19610 Arizona Alzheimer's Disease Core Center), the Arizona Department of Health Services (contract 211002, Arizona Alzheimer's Research Center), the Arizona Biomedical Research Commission (contracts 4001, 0011, 05-901 and 1001 to the Arizona Parkinson's Disease Consortium) and the Michael J. Fox Foundation for Parkinson's Research.

References

1. Klunk WE, Engler H, Nordberg A, et al. Imaging brain amyloid in Alzheimer's disease with Pittsburgh Compound-B. Annals of neurology. 2004; 55:306–319. [PubMed: 14991808]
2. Wong DF, Rosenberg PB, Zhou Y, et al. In vivo imaging of amyloid deposition in Alzheimer disease using the radioligand 18F-AV-45 (florbetapir [corrected] F 18). Journal of nuclear medicine : official publication, Society of Nuclear Medicine. 2010; 51:913–920.
3. Trojanowski JQ, Vandeerstichele H, Korecka M, et al. Update on the biomarker core of the Alzheimer's Disease Neuroimaging Initiative subjects. Alzheimer's & dementia : the journal of the Alzheimer's Association. 2010; 6:230–238.
4. Small GW, Kepe V, Ercoli LM, et al. PET of brain amyloid and tau in mild cognitive impairment. The New England journal of medicine. 2006; 355:2652–2663. [PubMed: 17182990]
5. Rowe CC, Ackerman U, Browne W, et al. Imaging of amyloid beta in Alzheimer's disease with 18F-BAY94-9172, a novel PET tracer: proof of mechanism. Lancet neurology. 2008; 7:129–135. [PubMed: 18191617]
6. Kung HF, Choi SR, Qu W, et al. 18F stilbenes and styrylpyridines for PET imaging of A beta plaques in Alzheimer's disease: a miniperspective. Journal of medicinal chemistry. 2010; 53:933–941. [PubMed: 19845387]
7. Koole M, Lewis DM, Buckley C, et al. Whole-body biodistribution and radiation dosimetry of 18F-GE067: a radioligand for in vivo brain amyloid imaging. Journal of nuclear medicine : official publication, Society of Nuclear Medicine. 2009; 50:818–822.
8. Clark CM, Schneider JA, Bedell BJ, et al. Use of florbetapir-PET for imaging beta-amyloid pathology. JAMA : the journal of the American Medical Association. 2011; 305:275–283. [PubMed: 21245183]
9. Jureus A, Swahn BM, Sandell J, et al. Characterization of AZD4694, a novel fluorinated Abeta plaque neuroimaging PET radioligand. Journal of neurochemistry. 2010; 114:784–794. [PubMed: 20477945]
10. Cselenyi Z, Jonhagen ME, Forsberg A, et al. Clinical Validation of 18F-AZD4694, an Amyloid-beta-Specific PET Radioligand. Journal of nuclear medicine : official publication, Society of Nuclear Medicine. 2012; 53:415–424.
11. Clark CM, Pontecorvo MJ, Beach TG, et al. Cerebral PET with florbetapir compared with neuropathology at autopsy for detection of neuritic amyloid-beta plaques: a prospective cohort study. Lancet neurology. 2012; 11(8):669–678. [PubMed: 22749065]
12. FDA Approves 18F-Florbetapir PET Agent. Journal of nuclear medicine : official publication, Society of Nuclear Medicine. 2012; 53:15N.

13. Beach TG, Monsell SE, Phillips LE, et al. Accuracy of the clinical diagnosis of Alzheimer disease at National Institute on Aging Alzheimer Disease Centers, 2005–2010. Journal of neuropathology and experimental neurology. 2012; 71:266–273. [PubMed: 22437338]
14. McKeith IG, Dickson DW, Lowe J, et al. Diagnosis and management of dementia with Lewy bodies: third report of the DLB Consortium. Neurology. 2005; 65:1863–1872. [PubMed: 16237129]
15. Consensus recommendations for the postmortem diagnosis of Alzheimer's disease. The National Institute on Aging, and Reagan Institute Working Group on Diagnostic Criteria for the Neuropathological Assessment of Alzheimer's Disease. Neurobiology of aging. 1997; 18:S1–S2. [PubMed: 9330978]
16. Duyckaerts C, Delatour B, Potier MC. Classification and basic pathology of Alzheimer disease. Acta neuropathologica. 2009; 118:5–36. [PubMed: 19381658]
17. Nelson PT, Jicha GA, Schmitt FA, et al. Clinicopathologic correlations in a large Alzheimer disease center autopsy cohort: neuritic plaques and neurofibrillary tangles "do count" when staging disease severity. Journal of neuropathology and experimental neurology. 2007; 66:1136–1146. [PubMed: 18090922]
18. Schneider JA, Arvanitakis Z, Bang W, et al. Mixed brain pathologies account for most dementia cases in community-dwelling older persons. Neurology. 2007; 69:2197–2204. [PubMed: 17568013]
19. Tsuang D, Simpson KL, Li G, et al. Evaluation of selection bias in an incident-based dementia autopsy case series. Alzheimer disease and associated disorders. 2005; 19:67–73. [PubMed: 15942323]
20. Beach TG, Sue LI, Walker DG, et al. The Sun Health Research Institute Brain Donation Program: description and experience, 1987–2007. Cell and tissue banking. 2008; 9:229–245. [PubMed: 18347928]
21. Zehntner SP, Chakravarty MM, Bolovan RJ, et al. Synergistic tissue counterstaining and image segmentation techniques for accurate, quantitative immunohistochemistry. The journal of histochemistry and cytochemistry : official journal of the Histochemistry Society. 2008; 56:873–880. [PubMed: 18574255]
22. Mirra SS, Heyman A, McKeel D, et al. The Consortium to Establish a Registry for Alzheimer's Disease (CERAD). Part II. Standardization of the neuropathologic assessment of Alzheimer's disease. Neurology. 1991; 41:479–486. [PubMed: 2011243]
23. Hyman BT, Trojanowski JQ. Consensus recommendations for the postmortem diagnosis of Alzheimer disease from the National Institute on Aging and the Reagan Institute Working Group on diagnostic criteria for the neuropathological assessment of Alzheimer disease. Journal of neuropathology and experimental neurology. 1997; 56:1095–1097. [PubMed: 9329452]
24. Thal DR, Rub U, Orantes M, et al. Phases of A beta-deposition in the human brain and its relevance for the development of AD. Neurology. 2002; 58:1791–1800. [PubMed: 12084879]
25. Braak H, Braak E. Neuropathological stageing of Alzheimer-related changes. Acta neuropathologica. 1991; 82:239–259. [PubMed: 1759558]
26. Sabbagh MN, Sandhu SS, Farlow MR, et al. Correlation of clinical features with argyrophilic grains at autopsy. Alzheimer disease and associated disorders. 2009; 23:229–233. [PubMed: 19812464]
27. Josephs KA, Whitwell JL, Parisi JE, et al. Argyrophilic grains: a distinct disease or an additive pathology? Neurobiology of aging. 2008; 29:566–573. [PubMed: 17188783]
28. Beach TG, Adler CH, Lue L, et al. Unified staging system for Lewy body disorders: correlation with nigrostriatal degeneration, cognitive impairment and motor dysfunction. Acta neuropathologica. 2009; 117:613–634. [PubMed: 19399512]
29. Obi K, Akiyama H, Kondo H, et al. Relationship of phosphorylated alpha-synuclein and tau accumulation to Abeta deposition in the cerebral cortex of dementia with Lewy bodies. Experimental neurology. 2008; 210:409–420. [PubMed: 18164295]
30. Hasegawa M, Arai T, Nonaka T, et al. Phosphorylated TDP-43 in frontotemporal lobar degeneration and amyotrophic lateral sclerosis. Annals of neurology. 2008; 64:60–70. [PubMed: 18546284]

31. Roman GC, Tatemichi TK, Erkinjuntti T, et al. Vascular dementia: diagnostic criteria for research studies. Report of the NINDS-AIREN International Workshop. Neurology. 1993; 43:250–260. [PubMed: 8094895]
32. Joshi AD, Pontecorvo MJ, Clark CM, et al. Performance characteristics of amyloid PET with florbetapir F 18 in patients with alzheimer's disease and cognitively normal subjects. Journal of nuclear medicine : official publication, Society of Nuclear Medicine. 2012; 53:378–384.
33. Wilson AC, Dugger BN, Dickson DW, et al. TDP-43 in aging and Alzheimer's disease - a review. International journal of clinical and experimental pathology. 2011; 4:147–155. [PubMed: 21326809]
34. Brooks DJ. Imaging amyloid in Parkinson's disease dementia and dementia with Lewy bodies with positron emission tomography. Movement disorders : official journal of the Movement Disorder Society. 2009; 24(Suppl 2):S742–S747. [PubMed: 19877240]
35. Edison P, Rowe CC, Rinne JO, et al. Amyloid load in Parkinson's disease dementia and Lewy body dementia measured with [11C]PIB positron emission tomography. Journal of neurology, neurosurgery, and psychiatry. 2008; 79:1331–1338.
36. Kantarci K, Yang C, Schneider JA, et al. Ante mortem amyloid imaging and beta-amyloid pathology in a case with dementia with Lewy bodies. Neurobiology of aging. 2010
37. Foster ER, Campbell MC, Burack MA, et al. Amyloid imaging of Lewy body-associated disorders. Movement disorders : official journal of the Movement Disorder Society. 2010; 25:2516–2523. [PubMed: 20922808]
38. Rowe CC, Ng S, Ackermann U, et al. Imaging beta-amyloid burden in aging and dementia. Neurology. 2007; 68:1718–1725. [PubMed: 17502554]
39. Maetzler W, Liepelt I, Reimold M, et al. Cortical PIB binding in Lewy body disease is associated with Alzheimer-like characteristics. Neurobiology of disease. 2009; 34:107–112. [PubMed: 19162186]
40. Gomperts SN, Rentz DM, Moran E, et al. Imaging amyloid deposition in Lewy body diseases. Neurology. 2008; 71:903–910. [PubMed: 18794492]
41. Maetzler W, Reimold M, Liepelt I, et al. [11C]PIB binding in Parkinson's disease dementia. NeuroImage. 2008; 39:1027–1033. [PubMed: 18035558]
42. Armstrong RA, Cairns NJ, Lantos PL. The spatial patterns of Lewy bodies, senile plaques, and neurofibrillary tangles in dementia with Lewy bodies. Experimental neurology. 1998; 150:122–127. [PubMed: 9514834]
43. Berg L, McKeel DW Jr, Miller JP, et al. Clinicopathologic studies in cognitively healthy aging and Alzheimer's disease: relation of histologic markers to dementia severity, age, sex, and apolipoprotein E genotype. Archives of neurology. 1998; 55:326–335. [PubMed: 9520006]
44. Lockhart A, Lamb JR, Osredkar T, et al. PIB is a non-specific imaging marker of amyloid-beta (Abeta) peptide-related cerebral amyloidosis. Brain : a journal of neurology. 2007; 130:2607–2615. [PubMed: 17698496]
45. Jack CR Jr, Wiste HJ, Vemuri P, et al. Brain beta-amyloid measures and magnetic resonance imaging atrophy both predict time-to-progression from mild cognitive impairment to Alzheimer's disease. Brain : a journal of neurology. 2010; 133:3336–3348. [PubMed: 20935035]

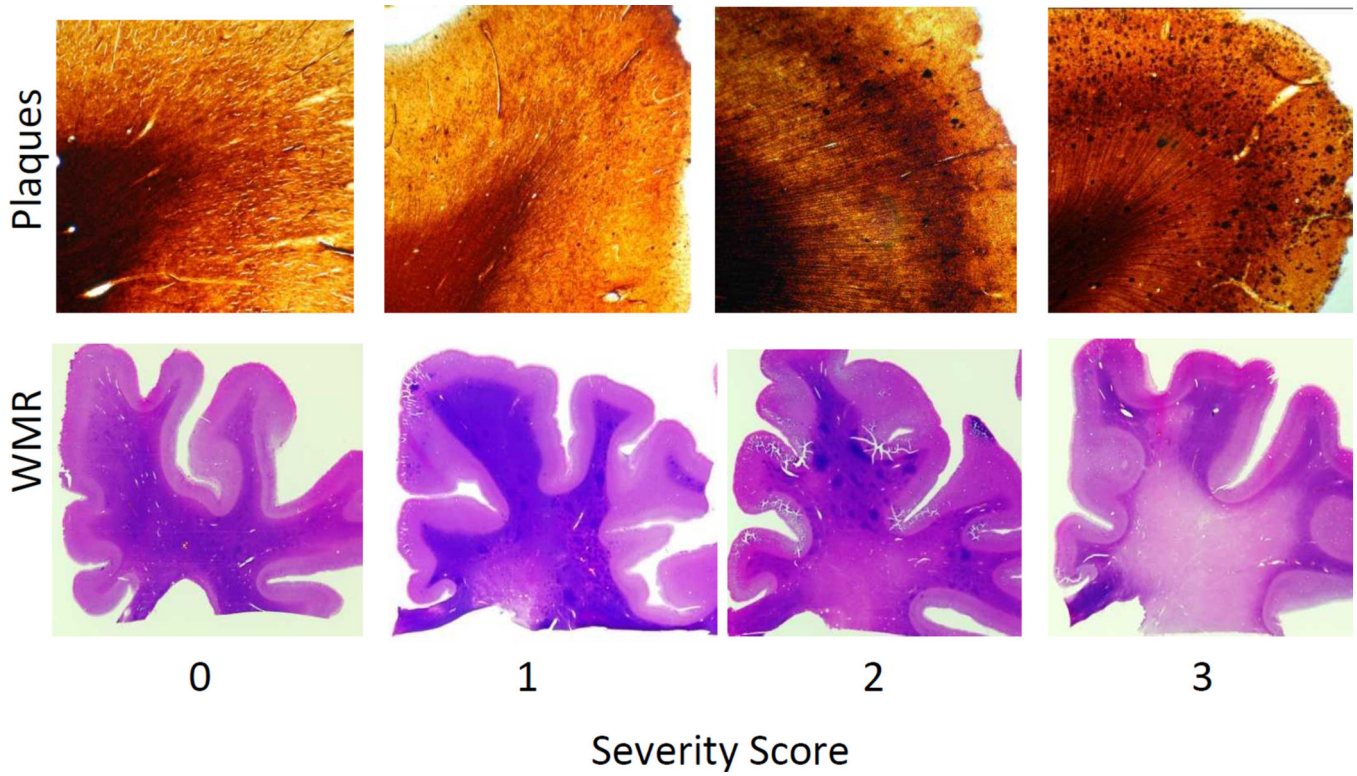

Figure 1.

Examples of severity scores given to plaque densities (top) and white matter rarefaction (WMR- bottom). Top: 80 μm sections of the superior frontal gyrus stained with the Campbell Switzer enhanced silver stain -from left to right: 0 - none, 1 - mild, 2 - moderate, and 3 - frequent plaque densities. Bottom: macro view of 80 μm sections of the frontal lobe stained with hematoxylin and eosin, WMR was scored as from left to right: 0 - none, 1 - mild, 2 - moderate, and 3 - severe. In this study, a case was defined as having significant WMR if it had a score of 2 or higher in one or more of the following lobes: frontal, parietal, temporal and occipital.

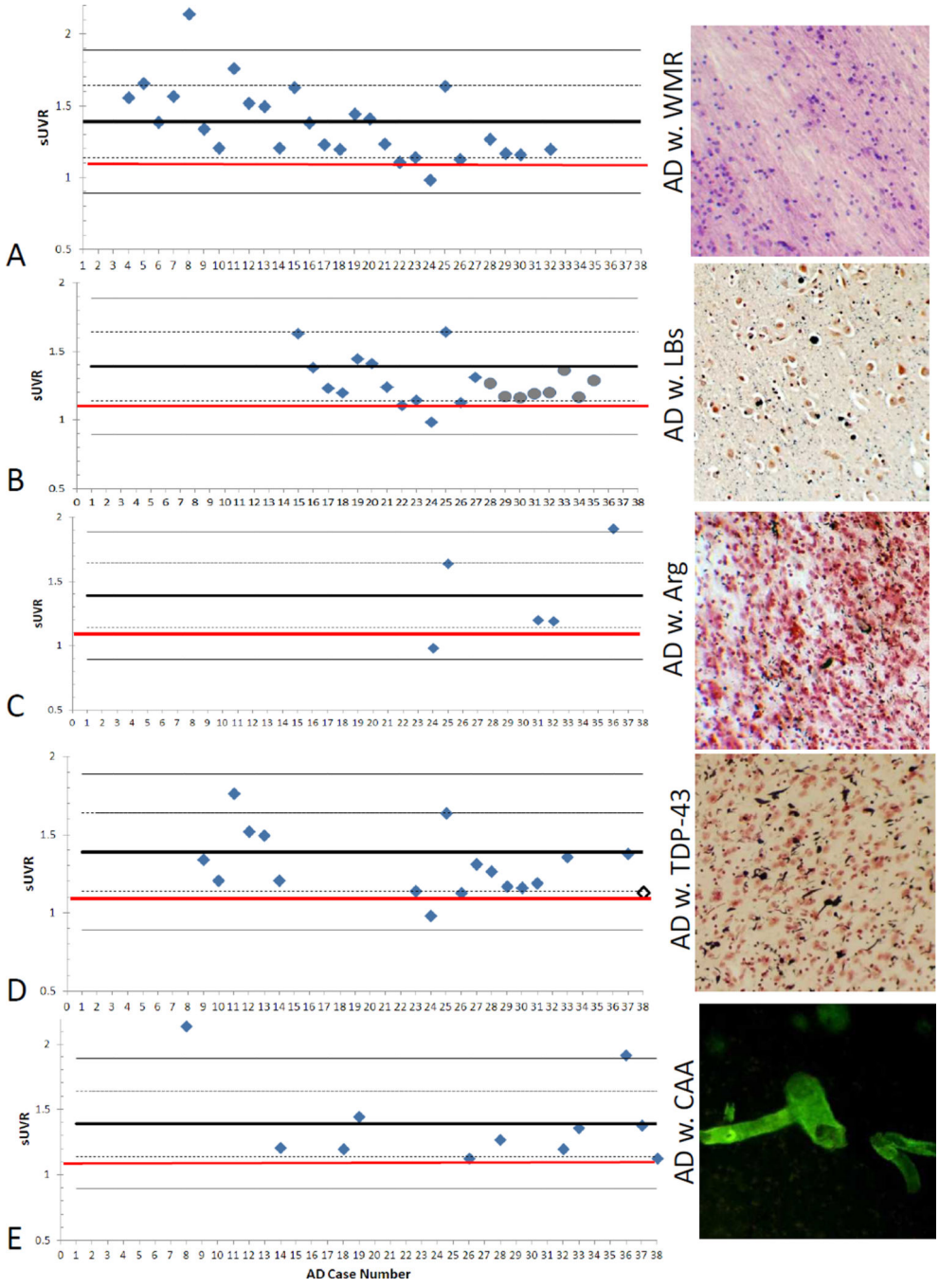

Figure 2.

Measures of average cortical amyloid load in AD subgroups with different concurrent pathologies. Left: Graphs demonstrating the variability of *in vivo* amyloid imaging measures for average cortical amyloid load, using the mean standard uptake value ratios (SUVr) for each AD subgroup. The thick black line on all graphs represents the mean of all AD cases, while the dashed and lighter lines represent one and two standard deviations from the mean, respectively. The red line at an SUVr value of 1.1. represents an adopted SUVr cut off between amyloid positive and negative (32). The x-axis numbers are the individual case

numbers as listed in Table 2. Right: photos taken at 10× of the respective pathologies. Panel **A**: AD with white matter rarefaction (WMR) – photo from an 80 μm section of parietal cortex white matter stained with hematoxylin and eosin. Panel **B**: AD with Lewy bodies (LBs-grey circles indicate clinicopathological diagnosis of DLB), photo from a 5 μm paraffin amygdala section stained immunohistochemically for phosphorylated α-synuclein (black) and counterstained with Neutral Red. Panel **C**: AD with argyrophilic grains (Arg), photo from an 80 μm section of amygdala stained with the Gallyas silver method. Panel **D**: AD with TDP-43 inclusions (white diamond indicates case with a clinicopathological diagnosis of FTLD-TDP-43 in addition to AD) ; photo taken from a 40 μm section of middle frontal gyrus that was immunohistochemically stained for phosphorylated TDP-43 (black) and counterstained with Neutral Red. Panel E: AD with severe cerebral amyloid angiopathy (CAA); photo from an 80 μm Thioflavin-S stained section of frontal cortex.

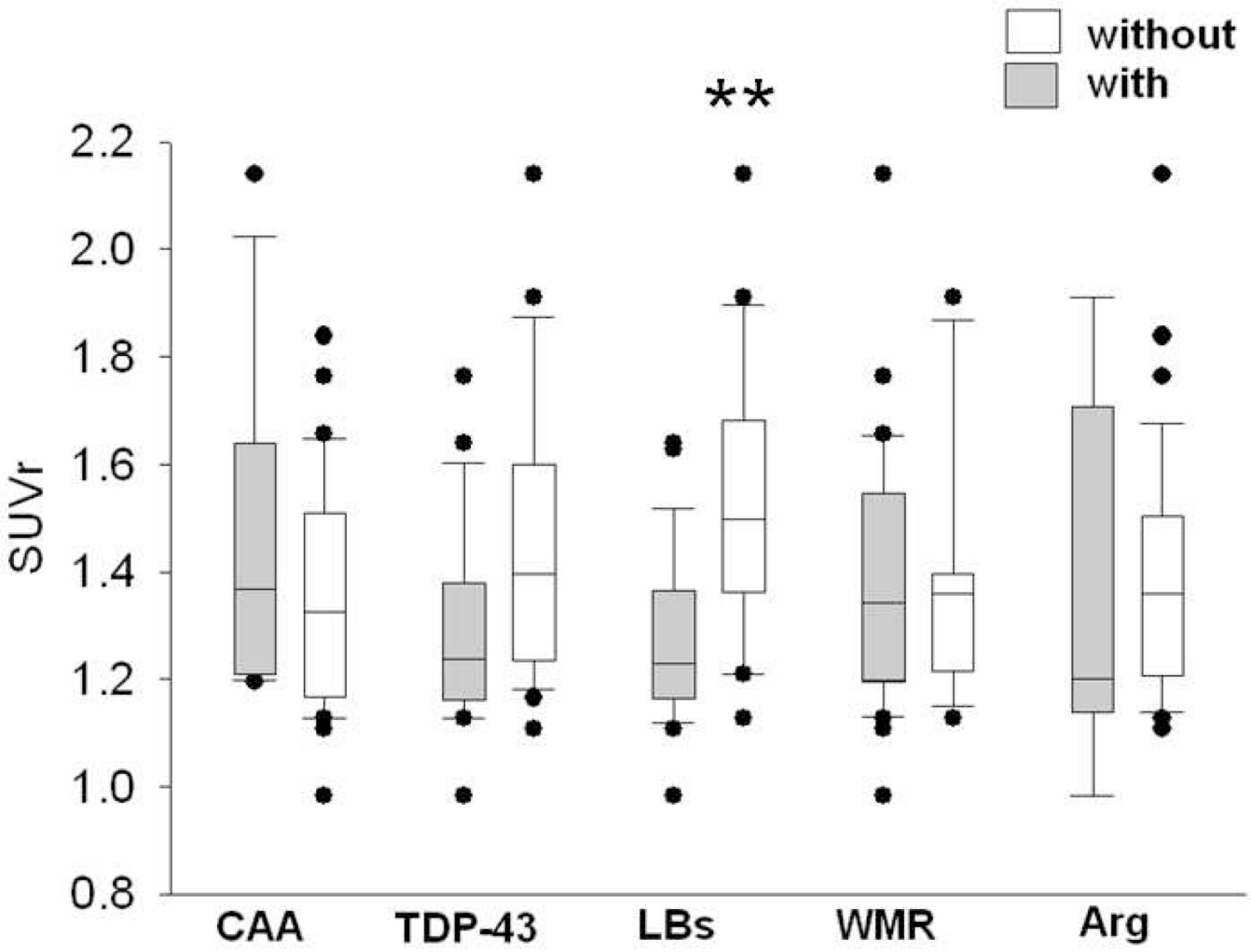

Fig. 3.

Box plots of median, 25th and 75th percentile of *in vivo* amyloid imaging measures for average cortical amyloid load of Alzheimer's disease cases using the standard uptake value ratios (SUVr) in subjects with presence (gray boxes) or absence (white boxes) of concurrent pathologies: (CAA; with N = 11; without N = 27), TDP-43 (with N = 18; without N = 20), LBs (with n = 21, without N = 17), WMR (with N = 27, without N = 11), and Arg (with N = 5, without N = 33). Whiskers above and below the box indicate the 90th and 10th percentiles. Utilizing the Mann-Whitney U-test, the only significantly different pairwise comparison was that comparing AD subjects with and without LBs (p = 0.002).

J Neuropathol Exp Neurol. Author manuscript; available in PMC 2015 January 01.

Table 1

Characteristics of AD subjects who received *in vivo*amyloid imaging. All subjects had frequent CERAD neuritic plaque densities. Also shown, for case with Lewy-type phosphorylated α-synuclein pathology, are the Unified Stages, (LB stages) according to published criteria (28).

Case	Age	gender	Braak NFT	Thal Stage	WMR+	CAA++	LB present/LB Stage	Arg	TDP	IHC	SUVR	Pathology Subset
1	91	F	VI	5	1	2	N	N	N	9.4	1.4	"Pure" AD
2	88	F	V	5	2	3	N	N	N	3.7	1.4	"Pure" AD
3	84	M	VI	5	1	6	N	N	N	7.4	1.8	"Pure" AD
4	86	F	V	4	2	1	N	N	N	5.4	1.6	WMR
5	84	M	V	5	6	5	N	N	N	8.8	1.7	WMR
6	89	F	IV	3	4	5	N	N	N	1.6	1.4	WMR
7	59	F	VI	5	5	5	N	N	N	10.4	1.6	WMR
8	80	M	V	5	4	9	N	N	N	9.6	2.1	WMR/CAA
9	67	F	V	5	5	2	N	N	Y	7.2	1.3	WMR/TDP
10	88	F	V	5	8	4	N	N	Y	1.6	1.2	WMR/TDP
11	91	F	V	5	10	0	N	N	Y	6.1	1.8	WMR/TDP
12	95	F	VI	5	10	1	N	N	Y	6.1	1.5	WMR/TDP
13	78	F	VI	5	8	4	N	N	Y	8.0	1.5	WMR/TDP
14	70	F	VI	5	11	12	N	N	Y	14.2	1.2	WMR/CAA/TDP
15	69	M	VI	5	9	0	Y / lll. Brainstem/Limbic	N	N	6.0	1.6	WMR/LBs
16	79	F	VI	5	6	5	Y / llb. Limbic	N	N	8.6	1.4	WMR/LBs
17	88	M	V	4	6	2	Y / llb. Limbic	N	N	4.8	1.2	WMR/LBs
18	76	M	VI	5	8	12	Y / llb. Limbic	N	N	7.4	1.2	WMR/CAA/LBs
19	86	F	VI	5	8	9	Y / llb. Limbic	N	N	3.7	1.4	WMR/CAA/LBs
20	67	F	VI	5	5	4	Y / llb. Limbic	N	N	8.8	1.4	WMR/LBs
21	85	F	VI	5	5	5	Y / l. Olfactory-Only	N	N	7.0	1.2	WMR/LBs
22	77	F	V	5	6	5	Y / llb. Limbic	N	N	6.9	1.1	WMR/LBs
23	96	F	V	5	4	5	Y / lll. Brainstem/Limbic	N	Y	3.6	1.1	WMR/LBs/TDP
24	104	F	IV	3	4	3	Y / llb. Limbic	Y	Y#	0.5	1.0	WMR/LBs/Arg/TDP
25	92	M	VI	5	9	10	Y / lll. Brainstem/Limbic	Y	Y#	1.4	1.6	WMR/CAA/LBs/Arg/TDP
26	103	F	V	5	5	6	Y / lll. Brainstem/Limbic	N	Y#	7.4	1.1	WMR/LBs/TDP
27	85	M	V	5	3	5	Y / llb. Limbic	N	Y	9.9	1.3	LBs/TDP

Case	Age	gender	Braak NFT	Thal Stage	WMR+	CAA++	LB present/LB Stage	Arg	TDP	IHC	SUVR	Pathology Subset
28	89	F	VI	5	12	8	Y/ lV. Neocortical*	N	Y	7.8	1.3	WMR/CAA/LBs/TDP
29	82	M	V	4	5	4	Y / lV. Neocortical*	N	Y	9.6	1.2	WMR/LBs/TDP
30	77	F	VI	5	8	3	Y / lV. Neocortical*	N	Y	5.8	1.2	WMR/LBs/TDP
31	81	M	IV	4	1	6	Y / lV. Neocortical*	Y	Y	4.4	1.2	LBs/Arg/TDP
32	81	F	VI	5	12	12	Y / lV. Neocortical*	Y	N	5.3	1.2	CAA/WMR/LBS/Arg
33	72	F	VI	5	3	12	Y / lV. Neocortical*	N	Y	5.3	1.4	CAA/LBs/TDP
34	78	M	IV	4	1	3	Y / llb. Limbic*	N	N	3.6	1.2	LBs
35	63	M	VI	5	1	7	Y / lV. Neocortical*	N	N	8.9	1.3	CAA/LBs
36	91	M	VI	5	3	12	N	Y	N	6.1	1.9	CAA/Arg
37	55	M	VI	5	1	12	N	N	Y	4.7	1.4	CAA/TRISOMY 21/TDP
38	72	M	II	3	0	0	N	N	Y	4.9	1.1	FTLD-TDP**

+WMR score is the sum of the parietal, temporal, frontal, and occipital lobes; each lobe was graded on a 0–3 scale (Fig 1). Those cases with a score of 2 or higher in one or more lobes were considered to have WMR in the pathology subset.

++The CAA score is the sum of the following cerebral lobes: parietal, temporal, frontal, and occipital which were graded on a 0–3 scale. As nearly our entire AD series had some degree of CAA (87%), we defined CAA in the pathology subset when one or more of the cerebral lobes had a severity score of 2 or higher.

*indicates pathology meeting criteria for diagnosis of dementia with Lewy bodies, #indicates pathology met criteria for diagnosis of hippocampal sclerosis.

**Case 38 contained diagnostic levels and distributions of TDP-43 deposits for FTLD-TDP.

Abbreviations: Arg = argyrophilic grains disease; CAA = cerebral amyloid angiopathy; CERAD=Consortium to Establish A Registry for Alzheimer's Disease; FTLD=frontotemporal lobar degeneration; LBs = Lewy bodies; NFT = neurofibrillary tangle; NP = neuritic plaque; TDP= TDP-43; WMR = white matter rarefaction; IHC = average percentage of cortical gray matter in the 6 cortical ROIs that was occupied by Aβ immunoreactivity; SUVr = standard uptake value ratio for the average cortical uptake of florbetapir divided by the average cerebellar uptake.

Table 2

Comparison of subject characteristics of AD groups, the non-demented group and the group with mild cognitive impairment (MCI).

	Non-Demented	MCI	All AD	AD w. WMR	AD w. LBs	AD w. CAA	AD w. Arg	AD w. TDP-43
N	12	5	38	27	21	11	5	18
Interval of Imaging till death (months); mean± SD	4.8±5.19	7.8±8.44	7.1±5.96	7.3 ±6 .0	7.0 ± 5.9	5.2 ± 5.5	6.4 ± 6.5	8.8 ± 6.8
Age at Death (years); mean ± SD	79± 13.3	71±18.2	82±11.2	83 ± 10.9	82 ± 10.7	78 ± 11.9	90 ± 9.5	83 ± 3.1
Gender ratio; (M:F)	9:3	4:1	15:23	7:20	9:12	5:6	3:2	6:12
Braak NFT stage; median (range)	III (I–IV)	I (I–IV)	VI (II–VI)*	VI (IV–VI)*	VI (IV–VI)*	VI (V–VI)*	VI (IV–VI)*	V (II–VI)*
Thal stage; median (range)	1 (0–3)	0 (0–2)	5 (3–5)*	5 (3–5)*	5 (3–5)*	5 (5)*	5 (3–5)*	5 (3–5)*
Average plaque density; median (range)	0 (0–3)	0 (0–3)	3 (3)*	3 (3)*	3 (3)*	3 (3)*	3 (3)*	3 (3)*
SUVr; mean (range)	1.0 (0.87–1.1)	1.0 (0.87–1.1)	1.4 (0.98–2.1)*	1.4 (0.98–2.1)*	1.3 (0.98–1.6)*	1.5 (1.2–2.1)*	1.4 (0.98–1.9)*	1.3 (0.98–1.76)*
Beta amyloid IHC; mean (range)	0.2 (0–1.1)	0.4 (0–1.1)	6.4 (0.5–14.2)*	6.4 (0.5–14.2)*	6.0 (0.5–9.9)*	6.8 (1.4–14.2)*	3.6 (0.5–6.1)*	6.0 (0.5–14.2)*

Statistical significantly was determined using Kruskal-Wallis test to test for the equality among normal, MCI and each of the AD groups respectively. The AD groups were not significantly different with respect to their AD-associated histopathological measures (Braak NFT stage, Thal stage, and average plaque density scores) or with respect to their *in vivo*(quantitative SUVr method) or postmortem (IHC) average cortical amyloid load estimates;

*significantly different from the normal control and MCI groups. There was considerable overlap amongst AD subgroup (as demonstrated in table 1).

Abbreviations: AD = Alzheimer's disease; NFT = neurofibrillary tangle; IHC = immunohistochemistry; SD = standard deviation; SUVr = standard uptake value ratio.

Table 3

Unadjusted p-values listed for SUVr and Amyloid β immunohistochemistry (IHC) comparisons among AD groups.

	AD w. WMR	AD w. LBs	AD w. CAA	AD w. Arg	AD w. TDP-43
AD w. WMR	n/a	0.14, 0.636	0.489, 0.770	0.856, 0.060	0.297, 0.683
AD w. LBs	0.14, 0.636	n/a	0.045, 0.499	0.696, 0.064	0.746, 1.000
AD w. CAA	0.489, 0.770	0.045, 0.499	n/a	0.394, 0.082	0.115, 0.573
AD w. Arg	0.856, 0.060	0.696, 0.064	0.394, 0.082	n/a	0.5, 0.139
AD w. TDP-43	0.297, 0.683	0.746, 1.000	0.115, 0.573	0.5, 0.139	n/a

p values for each comparison are listed in the following order SUVr, IHC